Pioneer. Adv. Mater. 2026, 1(2): 1-8 *DOI: 10.48308/piadm.2025.241717.1011*

Shahid Beheshti University

Pioneering Advances in Materials

Journal homepage: http://piadm.sbu.ac.ir ISSN: 3115-7114

Research paper

A Spacer-Thickness Tunable Terahertz Metasurface Absorber for Wide-Angle and Polarization-Insensitive Operation

Seyedeh Maryam Hosseini , ***Fazel Jahangiri****

Laser and Plasma Research Institute, Shahid Beheshti University, Tehran, Iran

**f_jahangiri@sbu.ac.ir*

Article info:

Article history:

Received: 26/09/2025

Accepted: 05/10/2025

Keywords: Metasurface, terahertz, polarization-insensitive, incident angle-insensitive, spacer-thickness tunable.

Abstract

Terahertz metasurfaces show great potential for communications, sensing, and imaging, but are often limited by complex designs, sensitivity to polarization and incident angle, and lack of tunability. This work addresses these challenges with a simple, compact, and efficient design. We design a terahertz metasurface perfect absorber with dual frequency selectivity and good incident angle compatibility using a gallium-doped ZnO resonator microring array separated from a copper ground plane by a GaAs spacer. The absorption properties of terahertz waves (0.1–10 THz) were simulated using full-wave electromagnetic theory. Simulations reveal two selective absorption peaks with absorption of 99.68% at 2.4463 THz and 99.84% at 7.8418 THz. The four-fold rotational symmetry ensures polarization insensitivity and stable performance across a broad range of incidence angles from 0° to 60°. Importantly, tuning the spacer thickness allows predictable adjustment in the number of absorption peaks without altering the resonator geometry. This versatile, easy-to-fabricate platform paves the way for economical and reliable terahertz devices like absorbers, filters, modulators, and sensors.

1. Introduction

The terahertz (THz) range spans frequencies from 0.1 to 10 THz, bridging the electronic and photonic domains [1]. This spectral range presents transformative opportunities for numerous applications, including high-speed wireless communications (such as 6G and beyond), non-destructive imaging, chemical fingerprinting, and biological sensing [2-4]. The full utilization of terahertz waves remains hindered by the limited availability of efficient, versatile, and cost-effective active devices capable of dynamic wavefront manipulation.

Metasurfaces, as two-dimensional arrays of engineered subwavelength meta-atoms, have emerged as a promising solution to the challenges of terahertz manipulation. These structures enable precise and flexible control over the amplitude, phase, and polarization of

electromagnetic waves, surpassing the capabilities of conventional metamaterials [5, 6]. Through tailored designs, metasurfaces have demonstrated remarkable capabilities in achieving functionalities such as anomalous beam steering, focusing, and absorption, all within ultrathin profiles [7].

Despite significant advancements, the practical implementation of terahertz metasurfaces is frequently limited by critical challenges. First, many sophisticated designs are highly susceptible to the polarization state of the incident wave, requiring specific linear or circular polarization for optimal operation. This sensitivity complicates system integration and restricts the metasurfaces' applicability in real-world environments [8, 9]. Second, their performance often deteriorates significantly at oblique incidence angles, limiting effective operation to near-normal incidence and restricting their applicability [10].

Finally, efforts to achieve dynamic tunability result in highly complex geometries incorporating materials such as graphene [11]. These additions introduce challenges, including fabrication complexity, increased losses, and higher costs.

This study presents a minimalist terahertz metasurface design embodying four essential characteristics: polarization insensitivity, wide-angle stability, straightforward tunability, and structural simplicity.

The design consists of an array of gallium-doped ZnO microring resonators placed above a continuous copper ground plane, separated by a GaAs spacer, forming a dual-band perfect absorber. The absorber's high-efficiency performance is elucidated through impedance matching principles and effective parameter analysis. Its structure symmetry ensures polarization-independent operation. The absorber has demonstrated insensitivity across a broad range of incidence angles.

Notably, the spacer layer thickness serves as a sole tuning parameter, enabling predictable and significant enhancement of absorption peaks by simple adjustment without modifying the resonator geometry. This post-fabrication tuning approach is both cost-effective and practical, as it circumvents the need for complex active materials and facilitates easier fabrication.

2. Design and simulation

The proposed THz absorber is composed of square-shaped unit cells with three distinct layers, shown in Fig. 1: a top layer with two gallium-doped ZnO (GZO) rings ($t_{GZO} = 0.49\ \mu m$ thick), an h=8 μm thick GaAs middle layer (loss tangent of 0.006 and a relative permittivity of 12.94), and a $t_{Cu} = 1\ \mu m$ thick copper ground plane bottom layer (frequency-independent conductivity of $5.8 \times 10^7\ S/m$) modeled as a lossy metal type. The GZO dielectric response in the THz region is described by the Drude model [12] via $\varepsilon(\omega) = \varepsilon_{DC} - \omega_p^2/(\omega^2 + i\gamma\omega)$, where $\varepsilon_{DC} = 7.46$ is the static dielectric constant. For the GZO film with a thickness of 0.49 μm, the plasma and the collision frequencies are $\gamma = 7.04 \times 10^{14}\ rad/s$ and $\omega_p = 6.96 \times 10^{14}\ rad/s$, respectively [12].

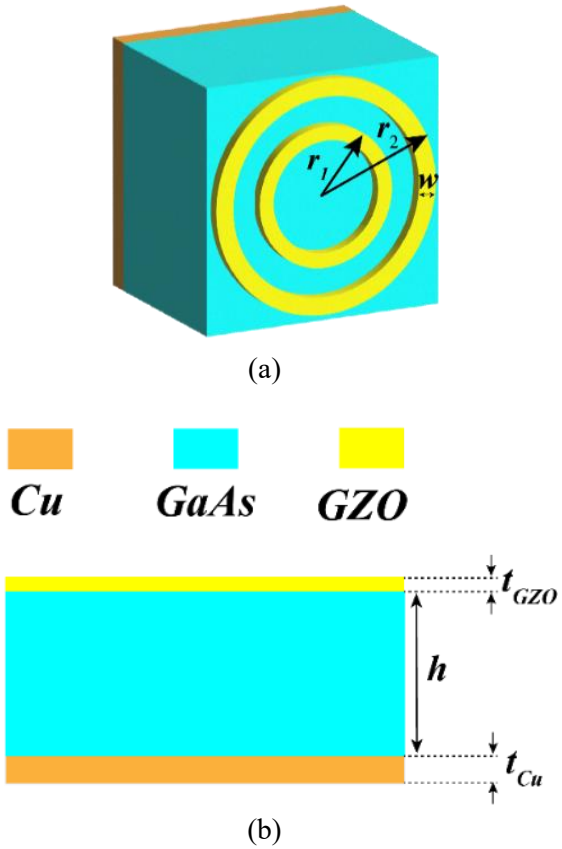

Fig. 1. (a) Three-dimensional, and (b) top view schematics of the absorber.

The unit cell period is P = 8 μm, and the optimized dimensions are: r_1=2 μm, r_2 = 3.9 μm, and w= 0.6 μm.

The electromagnetic response of the proposed THz absorber was simulated using CST Microwave Studio 2021 over 0.1 to 10 THz. The absorption was calculated from the S-parameter as $A(\omega) = 1 - R(\omega) - T(\omega)$, where $R(\omega) = |S_{11}(\omega)|^2$ and $T(\omega) = |S_{21}(\omega)|^2$ represent the reflection and transmission, respectively. Since the metal ground plane thickness exceeds the THz skin depth, the transmission $T(\omega)$ is zero. So, absorption $A(\omega)$ is given by $A(\omega) = 1 - |S_{11}(\omega)|^2$.

3. Results and discussions

Figure 2(a) shows the absorption spectra for transverse-electric (TE, electric field along x-axis) and transverse-magnetic (TM, electric field along y-axis) polarizations at normal incidence, which overlap perfectly.

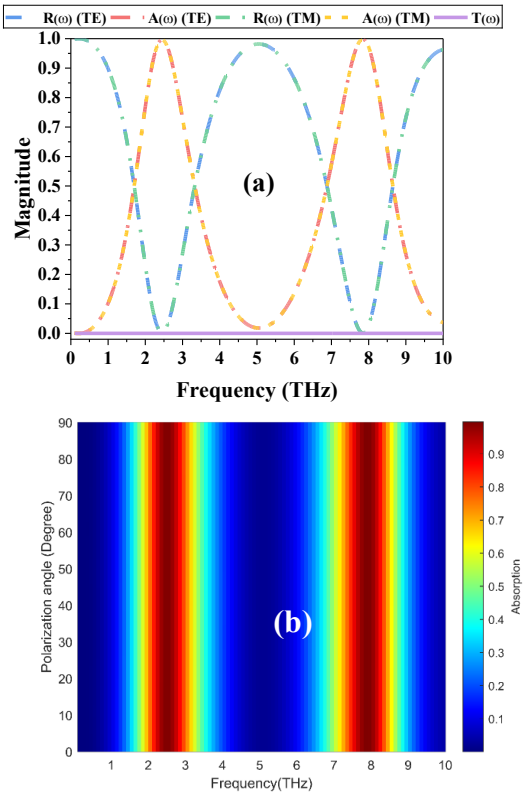

Fig. 2. (a) The reflection, absorption, and transmission spectra of the absorber. (b) The color diagram of the absorption spectrum with different polarization angles.

Two near-perfect absorption peaks appear at $f_1 = 2.4463\,THz$ and $f_2 = 7.8418\,THz$, with maximum absorption values of 99.68% and 99.84%, respectively. Figure 2(b) illustrates the absorption intensity for polarization angles from 0° to 90° in 10° increments, demonstrating polarization insensitivity due to the design's symmetry.

The large-angle absorption is crucial for assessing the absorber's practical performance. Figures 3(a) and 3(b) show absorption spectra at different incident angles for TE and TM polarizations. The absorber's unit structure, due to its multi-resonant ring design [13], produces similar angle-dependent absorption for both polarizations. Absorption remains above 85% up to a 60° incidence angle, demonstrating strong large-angle performance with consistent absorption in both polarizations.

An ideal absorber maintains stable absorption and resonant frequency regardless of polarization or incidence angle, though minor variations are difficult to control. Figure 3(c) presents maximum absorption at resonant frequencies f_1 and f_2 versus incidence angle for TE and TM modes. Slight differences appear at larger angles (45°–60°), likely due to impedance mismatch. Overall, the metasurface absorber performs well (up to 85%) over a broad range of angles. Small shifts of the resonant frequencies toward higher values occur in both TE and TM polarizations as the incidence angle increases, as shown in Figs. 3(d) and 3(e). The f_1 resonance shifts by 0.0297 THz at 35° for TE and 25° for TM polarizations, while the f_2 resonance shifts by 0.0297 THz at 18° for both polarizations. These shifts are minor compared to the typical spectral resolution (~0.03 THz~0.1 cm^{-1}) of terahertz time-domain spectrometers [14], confirming the absorber's robustness and reliable performance.

Impedance matching theory explains the perfect absorption mechanism. Maximum absorption occurs when the absorber's impedance matches free space ($Z = Z_0$). The relative impedance Z_r of the proposed absorber and its absorption under normal incidence are defined by the following relations:

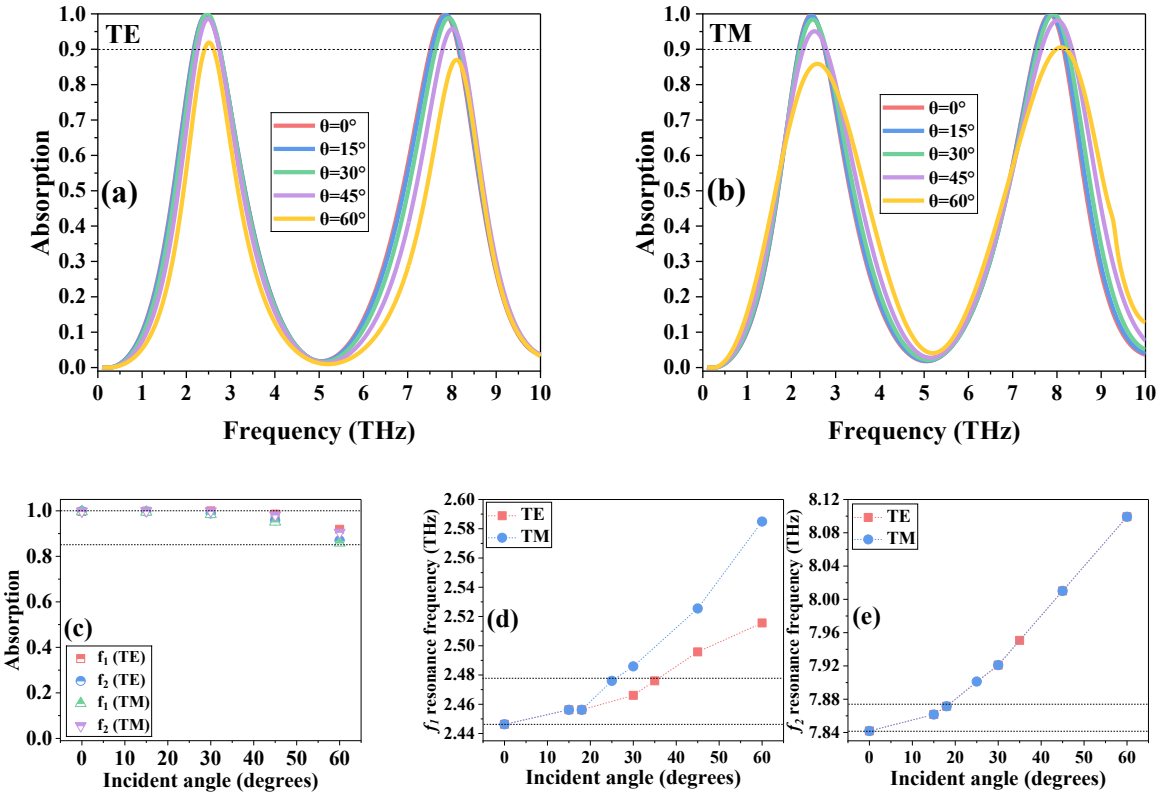

Fig. 3. The absorption spectra under different incident angles for (a) TE polarization, and (b) TM polarization. (c) Maximum absorption spectrum as a function of the incidence angle at the resonance frequencies, 2.4463 THz and 7.8418 THz, for TE and TM polarizations. Shift in (d) f_1, and (e) f_2 resonant frequencies with respect to the incidence angle for TE and TM polarizations.

$$Z_r = \sqrt{\frac{\mu}{\varepsilon}} = \frac{Z}{Z_0} = \sqrt{\frac{(1+S_{11}(\omega))^2-(S_{21}(\omega))^2}{(1-S_{11}(\omega))^2-(S_{21}(\omega))^2}} \qquad (1)$$

Here, Z and Z_0 are the effective impedances of the absorber and free space, while $S_{11}(\omega)$ and $S_{21}(\omega)$ are the reflection and transmission coefficients from CST simulations. Figure 4(a) shows the real and imaginary parts of the relative impedance for the proposed absorber under normal incidence (TE polarization). At 2.4463 THz and 7.8417 THz, the real part approaches unity and the imaginary part is near zero, with relative impedances Z_r=0.995−j0.113 and Z_r=0.978−j0.075, respectively. This satisfies the impedance matching condition, enabling perfect absorption. The effective permittivity (ε_{eff}) and permeability (μ_{eff}) were extracted using the method in Ref. [15] to identify resonances with strong electromagnetic confinement. For TE polarization (Fig. 4b), at both resonant frequencies, ε_{eff} is positive while μ_{eff} is negative, indicating magnetic resonance with μ-negative behavior. This negative permeability confirms the presence of localized magnetic fields [16]. Varying the spacer thickness offers an efficient approach to tune the frequency position, intensity, and number of absorption peaks without modifying the lateral geometry of the resonators. This capability is especially valuable for engineering multi-band absorbers tailored for selective and broadband terahertz applications. As illustrated in Figs. 5 (a–d), increasing the GaAs spacer thickness from 8 to 12, 16, and 20 μm results in a corresponding increase in the number of absorption peaks from 2 to 3, 4, and 5. This effect arises because spacer thickness can alter both the amplitude and phase relationships of internal waves, enabling the

excitation of additional localized resonant modes [17].

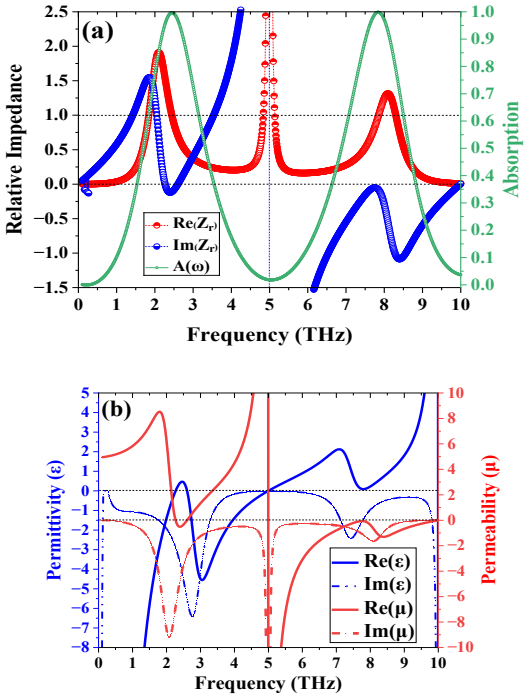

Fig. 4. Effective parameters analysis. Real and imaginary parts of (a) relative impedance, and (c) effective permittivity and permeability.

Consequently, multiple absorption peaks emerge across the terahertz spectrum, enhancing absorber functionality by broadening the operational frequency range for targeted applications. This phenomenon aligns with recent findings showing that spacer thickness critically influences near-field interlayer coupling and electromagnetic interference effects, which govern the absorber's resonant behavior and spectral response.

Table I summarizes the absorption characteristics of the proposed absorber as a function of dielectric spacer thickness under normal incidence for TE polarization. In addition, Figs. 6 (a–d) present color maps of the absorption spectra at varying incident angles for spacer thicknesses of 12 μm, 16 μm, and 20 μm. The absorber maintains over 80% absorption even as the dielectric thickness and incident angle increase. Notably, the absorption performance surpasses previously reported results [18-21].

Table I. Absorption performance of the proposed absorber under varying spacer thicknesses for TE polarization.

GaAs thickness (μm)	No. of peaks	Resonance frequencies	Maximum absorption (%)
***h*=8**	2	2.4463	99.68
		7.8418	99.84
***h*=12**	3	1.6264	99.19
		5.1688	99.65
		8.713	99.87
***h*=16**	4	1.2088	96.79
		3.8521	99.78
		6.5053	99.29
		9.1387	99.68
***h*=20**	5	0.9712	93.6
		3.07	99.99
		5.1886	99.41
		7.2973	99.35
		9.3961	99.71

So, our design has key advantages. First, the resonator structure is simple and single-layered. Unlike many high-performance metasurfaces that depend on complex multi-layered resonators [22], nested structures [23, 24], or intricately detailed split-ring resonators [25] pushing lithographic limits, our design employs a microring array with a single continuous geometric pattern. This significantly reduces fabrication challenges, avoiding the difficulties associated with numerous sharp corners [26], ultra-fine gaps [27], or multi-material stacks [28]. Second, the feature sizes and periodicity of our microrings fall well within the resolution of standard photolithography techniques. This contrasts with designs requiring costly and time-consuming methods such as electron-beam lithography to achieve sub-micron features [29]. Third, the fabrication process is fully planar. The structure is realized through a straightforward sequence of depositing a copper ground plane, a GaAs spacer layer, and a GZO top resonator layer.

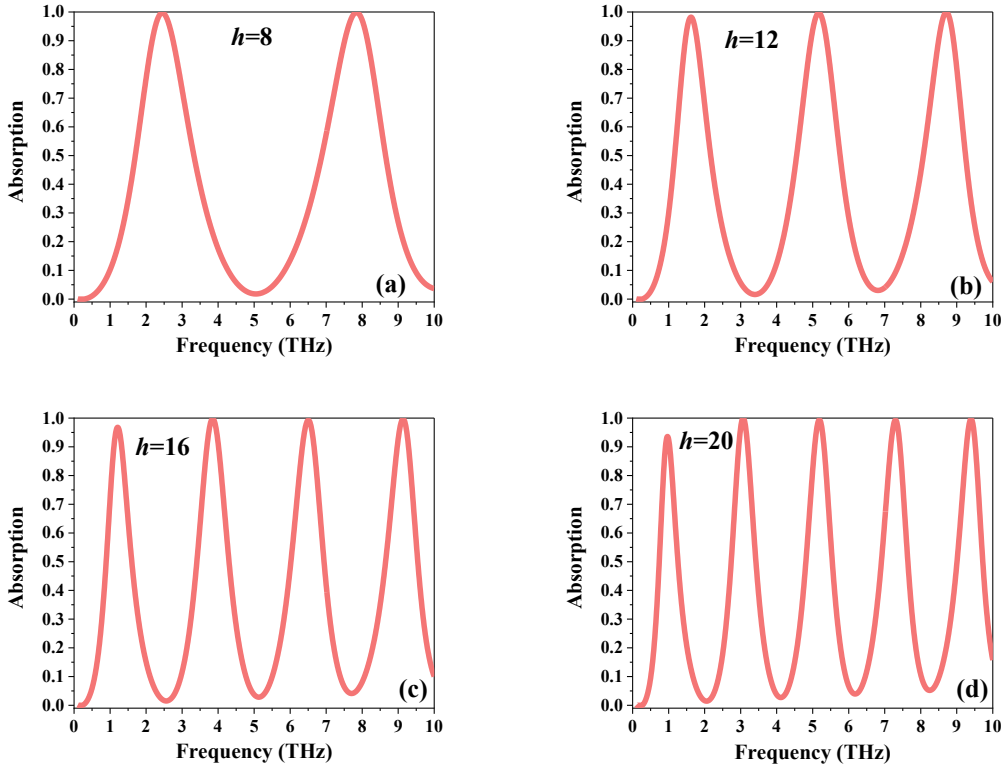

Fig. 5. Dependence of absorption spectrum on dielectric spacer thickness (*h*) for TE polarization.

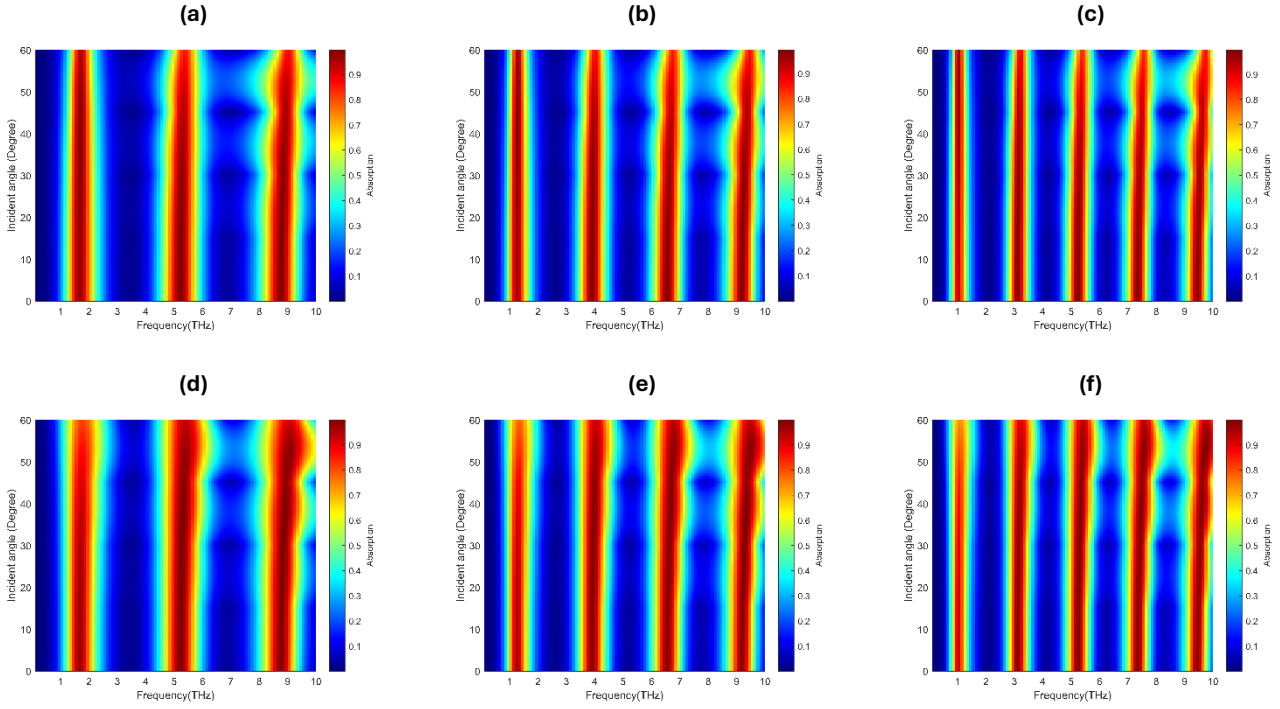

Fig. 6. The color maps of absorption spectra under different incident angles for spacer thicknesses h=12 μm, h=16 μm, and h=20 μm: panels (a–c) show results for TE polarization, and panels (d–f) for TM polarization.

This approach eliminates the need for complex three-dimensional structuring [7], precise alignment between multiple resonant layers, or challenging transfer steps required for emerging materials like graphene [30]. Finally, the design offers tunability without the need for redesigning the resonator pattern. As detailed in the present work, tuning is accomplished by varying the spacer thickness—a parameter readily controlled during standard deposition processes. This is considerably simpler than approaches requiring the fabrication of distinct resonator patterns [31] for each target frequency.

4. Conclusion

In conclusion, we have presented a minimalist design of a dual-band terahertz metasurface absorber based on gallium-doped ZnO microrings. Numerical simulations demonstrate near-perfect absorption at two distinct frequencies, 2.4463 THz and 7.8418 THz. A detailed analysis leveraging impedance matching theory and effective medium parameters provides insight into the physical mechanisms responsible for this perfect absorption. The absorber exhibits remarkable robustness against variations in incidence angle (0°–60°) and polarization angles, highlighting its wide-angle and polarization-insensitive performance. Moreover, by tuning the thickness of the GaAs spacer—a fabrication-friendly parameter—the number of absorption peaks can be predictably increased without modifying the resonator geometry. This straightforward design, combined with the choice of materials, simplifies fabrication and offers practical advantages. While this study focuses on numerical investigation, it provides valuable technical insights for the design and potential realization of efficient terahertz metasurface absorbers.

Disclosures

The authors declare no conflicts of interest.

References

1. *P. U. Jepsen, D. G. Cooke, and M. Koch, "Terahertz spectroscopy and imaging–Modern techniques and applications," Laser & Photonics Reviews, vol. 5, no. 1, pp. 124–166, 2011.*
2. *S. Koenig et al., "Wireless sub-THz communication system with high data rate," Nature photonics, vol. 7, no. 12, pp. 977–981, 2013.*
3. *M. Tonouchi, "Cutting-edge terahertz technology," Nature photonics, vol. 1, no. 2, pp. 97–105, 2007.*
4. *T. Amini, F. Jahangiri, Z. Ameri, and M. A. Hemmatian, "A review of feasible applications of THz waves in medical diagnostics and treatments," Journal of Lasers in Medical Sciences, vol. 12, p. e92, 2021.*
5. *N. Yu and F. Capasso, "Flat optics with designer metasurfaces," Nature materials, vol. 13, no. 2, pp. 139–150, 2014.*
6. *S. B. Glybovski, S. A. Tretyakov, P. A. Belov, Y. S. Kivshar, and C. R. Simovski, "Metasurfaces: From microwaves to visible," Physics reports, vol. 634, pp. 1–72, 2016.*
7. *H.-T. Chen, A. J. Taylor, and N. Yu, "A review of metasurfaces: physics and applications," Reports on progress in physics, vol. 79, no. 7, p. 076401, 2016.*
8. *M. K. T. Al-Nuaimi, W. Hong, and W. G. Whittow, "Aperiodic sunflower-like metasurface for diffusive scattering and RCS reduction," IEEE Antennas and Wireless Propagation Letters, vol. 19, no. 7, pp. 1048–1052, 2020.*
9. *D. Wen et al., "Helicity multiplexed broadband metasurface holograms," Nature communications, vol. 6, no. 1, p. 8241, 2015.*
10. *K. Aliqab, A. Armghan, and M. Alsharari, "Polarization insensitive and wideband terahertz absorber using high-impedance resistive material of RuO2," Scientific Reports, vol. 14, no. 1, p. 19149, 2024.*
11. *H.-T. Chen, W. J. Padilla, J. M. Zide, A. C. Gossard, A. J. Taylor, and R. D. Averitt, "Active terahertz metamaterial devices," Nature, vol. 444, no. 7119, pp. 597–600, 2006.*

12. *J. Tang et al., "Determination of carrier concentration dependent electron effective mass and scattering time of n-ZnO thin film by terahertz time domain spectroscopy," Journal of Applied Physics, vol. 115, no. 3, 2014.*
13. *G. Wu, X. Jiao, Y. Wang, Z. Zhao, Y. Wang, and J. Liu, "Ultra-wideband tunable metamaterial perfect absorber based on vanadium dioxide," Optics Express, vol. 29, no. 2, pp. 2703–2711, 2021.*
14. *P. Han, M. Tani, M. Usami, S. Kono, R. Kersting, and X.-C. Zhang, "A direct comparison between terahertz time-domain spectroscopy and far-infrared Fourier transform spectroscopy," Journal of Applied Physics, vol. 89, no. 4, pp. 2357–2359, 2001.*
15. *S. M. Hosseini, F. Jahangiri, and H. Latifi, "Bandwidth improvement in copper-based terahertz metamaterial absorbers by structural engineering," Optics Express, vol. 33, no. 17, pp. 35336–35351, 2025.*
16. *P. A. Huidobro et al., "Magnetic localized surface plasmons," Physical Review X, vol. 4, no. 2, p. 021003, 2014.*
17. *Y. Wang, Z. Cui, D. Zhu, and L. Yue, "Composite metamaterials for THz perfect absorption," physica status solidi (a), vol. 216, no. 6, p. 1800940, 2019.*
18. *M. Raza, X. Li, C. Mao, F. Liu, H. He, and W. Wu, "A polarization-insensitive, vanadium dioxide-based dynamically tunable multiband terahertz metamaterial absorber," Materials, vol. 17, no. 8, p. 1757, 2024.*
19. *Z. Ren et al., "A switchable terahertz metamaterial absorber between ultra-broadband and dual bands," Frontiers in Physics, vol. 11, p. 1227013, 2023.*
20. *Y. Zhang et al., "Five-band terahertz perfect absorber based on metal layer–coupled dielectric metamaterial," Plasmonics, vol. 14, no. 6, pp. 1621–1628, 2019.*
21. *Z. Chen et al., "Graphene multi-frequency broadband and ultra-broadband terahertz absorber based on surface plasmon resonance," Electronics, vol. 12, no. 12, p. 2655, 2023.*
22. *M. Masyukov, A. Vozianova, A. Grebenchukov, K. Gubaidullina, A. Zaitsev, and M. Khodzitsky, "Optically tunable terahertz chiral metasurface based on multi-layered graphene," Scientific reports, vol. 10, no. 1, p. 3157, 2020.*
23. *W. Pan, X. Yu, J. Zhang, and W. Zeng, "A novel design of broadband terahertz metamaterial absorber based on nested circle rings," IEEE Photonics Technology Letters, vol. 28, no. 21, pp. 2335–2338, 2016.*
24. *D. R. Chowdhury et al., "A broadband planar terahertz metamaterial with nested structure," Optics express, vol. 19, no. 17, pp. 15817–15823, 2011.*
25. *T. Ramachandran, M. R. I. Faruque, and K. Al-Mugren, "Symmetric left-handed split ring resonator metamaterial design for terahertz frequency applications," Scientific Reports, vol. 13, no. 1, p. 21828, 2023.*
26. *M. N. Hamza et al., "Design and validation of ultra-compact metamaterial-based biosensor for non-invasive cervical cancer diagnosis in terahertz regime," PloS one, vol. 20, no. 2, p. e0311431, 2025.*
27. *S. Asgari and T. Fabritius, "Multi-band terahertz anisotropic metamaterial absorber composed of graphene-based split square ring resonator array featuring two gaps and a connecting bar," Scientific Reports, vol. 14, no. 1, p. 7477, 2024.*
28. *C. Song et al., "Dual-band/ultra-broadband switchable terahertz metamaterial absorber based on vanadium dioxide and graphene," Optics Communications, vol. 530, p. 129027, 2023.*
29. *M. Seo et al., "Active terahertz nanoantennas based on VO2 phase transition," Nano letters, vol. 10, no. 6, pp. 2064–2068, 2010.*
30. *F. Bonaccorso, Z. Sun, T. Hasan, and A. C. Ferrari, "Graphene photonics and optoelectronics," Nature photonics, vol. 4, no. 9, pp. 611–622, 2010.*
31. *H. Tao et al., "A dual band terahertz metamaterial absorber," Journal of physics D: Applied physics, vol. 43, no. 22, p. 225102, 2010.*